Macromolecules
ARTICLE

Macromolecules **2009**, *42*, 5829–5842 **5829**
DOI: 10.1021/ma802709d

Microscopic Mechanisms of Strain Hardening in Glassy Polymers

Bart Vorselaars,*,†,‡ Alexey V. Lyulin,*,† and M. A. J. Michels†

†*Group Polymer Physics and Eindhoven Polymer Laboratories, Technische Universiteit Eindhoven, P.O. Box 513, 5600 MB Eindhoven, The Netherlands,* ‡*Department of Mathematics, University of Reading, Reading RG6 6AX, U.K., and* §*Dutch Polymer Institute, P.O. Box 902, 5600 AX Eindhoven, The Netherlands*

Received December 3, 2008; Revised Manuscript Received June 16, 2009

ABSTRACT: The mechanisms underlying the increase in stress for large mechanical strains of a polymer glass, quantified by the strain-hardening modulus, are still poorly understood. In the present paper we aim to elucidate this matter and present new mechanisms. Molecular-dynamics simulations of two polymers with very different strain-hardening moduli (polycarbonate and polystyrene) have been carried out. Nonaffine displacements occur because of steric hindrances and connectivity constraints. We argue that it is not necessary to introduce the concept of entanglements to understand strain hardening, but that hardening is rather coupled with the increase in the *rate* of nonaffine particle displacements. This rate increases faster for polycarbonate, which has the higher strain-hardening modulus. Also more nonaffine chain stretching is present for polycarbonate. It is shown that the inner distances of such a nonaffinely deformed chain can be well described by the inner distances of the worm-like chain, but with an effective stiffness length (equal to the Kuhn length for an infinite worm-like chain) that increases during deformation. It originates from the finite extensibility of the chain. In this way the increase in nonaffine particle displacement can be understood as resulting from an increase in the effective stiffness length of the perturbed chain during deformation, so that at larger strains a higher rate of plastic events in terms of nonaffine displacement is necessary, causing in turn the observed strain hardening in polymer glasses.

1. Introduction

Glassy polymeric materials harden for large strains, i.e., the stress needed to deform the material increases upon straining at large deformations. This is quantified by the strain-hardening modulus, which is the gradient of the line describing the relation between the stress and the Gaussian strain[1] in the postyield regime. If the strain-hardening effect is large enough, it can lead to a tough response of the polymeric material; the material breaks only after a significant plastic strain, as is the case for polycarbonate (PC). On the other hand, for polystyrene (PS), the strain-hardening effect is usually too weak, and consequently, that polymer breaks within a few percent of extension. Understanding the origin of the strain-hardening effect provides a strategy for tailor-made polymeric materials.

Unfortunately no well-accepted theory is available for the strain-hardening effect in the glassy state. The entropy-based rubber theory of elasticity[2,3] does describe some features of the strain-hardening effect (such as the functional dependence on strain), but drastically fails in predicting the absolute magnitude. For example, its prediction for polystyrene is short by 2 orders of magnitude.[4,5]

The failure of the rubber-elasticity theory is caused by the following obvious but important difference between a rubbery state and a glassy state. In a rubbery material, the various conformations of a polymer-chain part between cross-link points are easily accessible. These cross-link points can be either of a chemical nature (such as covalent bonds) or a physical nature (such as entanglements). In a glassy material, in contrast, a chain is surrounded by a glassy matrix and has a frozen-in conformation, because of energetic barriers between the various states. At rest it is trapped in a local energy minimum and when the sample is stretched and released afterward the strained state will not immediately relax toward the equilibrium state. Moreover, to deform the glassy material, the energetic barriers need to be surpassed and energy dissipation takes place. The work needed for this irreversible energy dissipation is delivered by a dissipative stress. This stress of dissipative nature is not present in the rubber-elasticity theory.

The dissipative nature of deforming a glassy polymer is confirmed by experiments and simulations. Experimentally it is found that for large strains (>15% for polycarbonate and >30% for polystyrene[6,1,7]) more work is converted into heat (i.e., dissipated) than into internal energy. Recent simulations of a polymer bead−spring model (known as the Kremer−Grest model[8]) also demonstrated that the dominant part of the stress at large strains is due to dissipation.[9,10]

One way of dealing with the dissipative nature of the deformation is to model the stress−strain relation in the strain-hardening regime by two contributions.[1,11] The first part is a constant dissipative stress σ_Y, due to the presence of energy barriers. The second is the strain-dependent part, which is thought to be described by rubber-elasticity theory and represents the strain-hardening effect. In this description the strain-hardening modulus is not affected by thermally activated processes.

However, experiments demonstrate that such a description for the strain-hardening part is invalid; also the strain-hardening modulus has characteristics of a thermally activated process. One observation is that the strain-hardening modulus decreases for higher temperatures.[12,13] This is in line with what one would expect for thermal activation. Another observation is that a higher strain rate leads to an increase in the strain-hardening modulus,[14] although for some polymers the dependency on strain rate is almost absent.[15] Also, this can be interpreted within the barrier-crossing picture. For higher deformation rates fewer

*Corresponding authors. E-mail: (B.V.) B.Vorselaars@reading.ac.uk; (A.V.L.) A.V.Lyulin@tue.nl.

Published on Web 07/15/2009

particles are able to overtake energetic barriers by a sufficient thermal fluctuation and therefore more particles need to be mechanically forced for crossing their barrier. Next to temperature and strain rate, the external pressure affects the strain-hardening modulus as well. A higher external pressure can lead to an increase in the strain-hardening modulus.[16] Again, this behavior is typical for thermally activated processes. All these three observations on the strain-hardening modulus are not present within the classical rubber theory.

What is the polymer-specific part of the strain-hardening modulus? Experiments[5] and simulations[17] show that this modulus is positively correlated with the entanglement density, and polymers with a larger Kuhn or persistence length often have a higher strain-hardening modulus.[12] It was even shown by molecular-dynamics (MD) simulations that if the persistence length of a polyethylene-like polymer is artificially increased by changing the trans-to-gauche ratio, the strain-hardening modulus of the resulting material increases as well.[18] That example illustrates that the strain-hardening modulus depends on the conformation of the chain, which is frozen in the glassy state.

Strain-hardening effects are already visible for relatively short chains. In our previous MD simulations of polystyrene[16] strain hardening was observed for chain lengths of 80 monomers, below the experimentally observed entanglement length of about 128−139 monomers.[19,20] Moreover, a doubling of the chain length to 160 monomers hardly changed the measured strain hardening modulus.[21] In that article the same finding was demonstrated for PC. While the entanglement length of PC is about 5 monomers,[20] systems with number of monomers per chain of both 10 and 64 were studied. Also here the strain hardening moduli were very similar in the investigated strain range. These findings are in accordance with simulations of a bead−spring polymer glass,[17] where it was demonstrated that there is a gradual increase in the strain-hardening modulus as a function of chain length for chains up to about the entanglement length. Longer chains effectively have the same strain hardening modulus. However, for very large strains the saturation occurs at an even longer chain length. In a different study of the same system, it was also observed that the strain hardening is more correlated with changes in the end-to-end distances of the polymer chains[9] than with changes in the macroscopic dimensions (i.e., the dimensions of the simulation box). For example, if the size of the sample is decreasing while the end-to-end distance of an individual chain does not, then the stress does not increase as well. Nevertheless, the same is probably also true for physically entangled rubbers.

Many results discussed so far are the result of MD simulations. Next to benefits of using MD simulations, one should also bear in mind the limitations of it, such as the limited range of length and time scales. MD simulations are usually carried out at much higher deformation rates than experimental ones. Nevertheless, the observed strain-hardening phenomena are similar to those acquired by mechanical experiments. This possibly originates from the observation that deep in the glassy state segmental relaxation times[22] greatly exceed both the experimental and the simulation time scales, so that for both situations one is looking in a time window where motions appear to be frozen and hence nonequilibrium phenomena associated with the glassy state can be observed.

The increase in stress for larger strains in combination with the dissipative nature of the stress in the strain-hardening regime suggest that there is an increase in the rate of energy dissipation, i.e., more energy per unit of strain is needed for more stretched samples. This picture is supported by a simulation study of a polymer bead−spring model.[9] It was observed that the dissipative stress increases with larger strain and that at zero temperature the stress was directly correlated to the rate of changes in Lennard-Jones (LJ) binding. Also the rate of conformational transitions is found to increase in the strain-hardening regime.[23] The reason for the rate increase, however, remains fuzzy. It has been observed that chains are pulling taut between entanglements,[10] but a physical picture underlying the increase in the rate is lacking.

There is not yet an answer on the question why the energy-dissipation rate is increasing with increasing strain (leading ultimately to an increase in the strain-hardening modulus). In this paper the aim is to shed light on that problem, by simulating two glassy polymers that vary greatly in their strain-hardening moduli, viz. polystyrene (PS) and polycarbonate (PC, of which the modulus is more than a factor of 2 higher[24]) and studying their behavior. Previous molecular-dynamics simulations of our group[16,21,25] have reproduced these experimental findings qualitatively, with a strain-hardening modulus of polystyrene that is much lower than that of polycarbonate. Such simulations open ways to look at the molecular level beyond the limitations of the currently available experimental techniques. In the present study we focus on indentifying the microscopic mechanisms responsible for the observed difference in the strain-hardening modulus. The study is different from previous ones in that it brings in new information about the role of chemical details that cannot be addressed by bead−spring models, that new quantities such as the rate of nonaffine displacements are analyzed and that the behavior of quantities during deformation are understood qualitatively and sometimes even quantitatively (such as the deformation of the intrachain distances).

The paper is organized in the following manner. Aspects of the simulations are given in section 2. Statistical quantities of the chain structure are introduced in section 3. The intrachain length scales for the two polymers can be found in the appendices A and B. In section 4, the stress−strain relation for both polymers PS and PC is presented and a difference in strain-hardening effect is observed, the effect being larger for PC. In section 5 the important role of nonaffinity is discussed. It is shown in section 5.3 that also the average nonaffine particle displacement, a measure for the amount of plasticity, is larger for PC. To ascribe strain hardening to it, more evidence is needed. This is done in section 5.4, where a measure for the rate of nonaffine displacements is calculated. It is found that this rate increases with larger strain, and that the increase is larger for PC. The nonaffine displacements of particles are caused by restrictions and hindrances, in particular from covalent and steric interactions. It is demonstrated in section 5.5 that, along with nonaffine self-displacements of particles, the inner length scales of a chain also change in a nonaffine way. This is because at the scale of the Kuhn length a chain cannot be stretched any further. However, due to the stretching of the chain at larger strains, the effective stiffness length of a perturbed chain increases, as shown in section 5.6. Such a larger stiffness length generates a larger rate of nonaffine particle displacements, thereby causing more energy dissipation and hence a larger stress, i.e., strain hardening. The conclusions based on these results are given in section 6.

2. Simulation Details

The united-atom force fields in use for the two polymers under investigation, PS and PC, have been used in our previous studies (see, e.g., refs 21, 16) and are given in refs 26, 27. Both monomer units are shown in Figure 1. The systems consist of 8 chains of 80 monomers each for polystyrene and 64 chains of 10 monomers each for polycarbonate. The total amount of united atoms per sample is therefore 5128 for polystyrene and 11904 for polycarbonate. One might think that these chain lengths are relatively short. However, as came forward from our previous[25] and other studies[17] and as mentioned in the introduction chains of this length show strain hardening comparable to much longer chains. Hence, the system under study should give relevant insight in hardening.

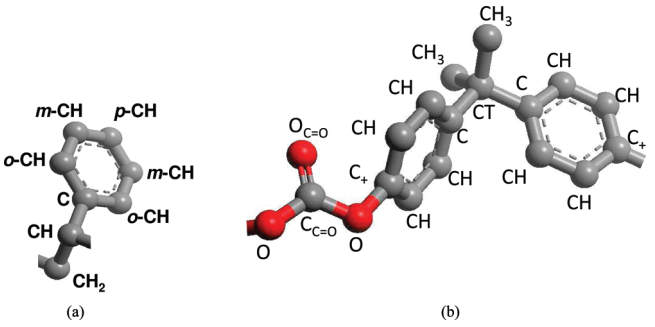

Figure 1. Monomer units of (a) PS and (b) PC.

The equilibration procedure for the two polymer melts is described in ref 26. The results to be presented for polystyrene are based on samples which are cooled from $T = 540$ K with a velocity of -0.01 K ps^{-1} until $T = 300$ K, about room temperature. Apart from the initial yield peak[16] the results based on these samples are very similar to those of the samples cooled with a temperature ramp of -0.1 K ps^{-1}, especially with respect to strain hardening. The polycarbonate samples have been cooled toward $T = 300$ K with a velocity of -0.05 K ps^{-1}. Initial densities at $T = 300$ K prior to deformation are 1.01 g cm^{-3} for polystyrene and 1.36 g cm^{-3} for polycarbonate.

For the simulated atactic-polystyrene system the glass-transition temperature is found to be around 380 K and for polycarbonate around 433 K,[21] so that both polymer systems are deep in the glassy state around room temperature. The presented deformation results are averaged over 15 samples for polystyrene and 5 samples for polycarbonate. For comparison isotropic, nondeforming, simulations at $T = 300$ are carried out with the same initial configuration. In that case results are averaged over 5 samples for both PS and PC.

The deformation protocol is identical to the one given in ref 16. Here we study only the uniaxial-stress extension molecular dynamics simulations, in which the box size in the extension direction increases with a velocity of $\dot{L}_{\|} = 0.01$ Å/ps, which corresponds to an initial deformation rate of roughly $(2-3) \times 10^8$ s^{-1}. Simulations with a constant deformation rate of 10^8 s^{-1} have been carried out as well, but they do not lead to different conclusions and are not presented here. The stress in the two other directions are controlled by the Berendsen barostat, in which the ratio of the relaxation time to the isothermal compressibility is taken to be $\tau_P/\beta = 0.011$ Pa s.

3. Intrachain Distances and Equilibrium Chain Structure

In the present study, the chain structure plays an important role. This structure will be quantified by measuring the intrachain length scales. We will therefore first introduce the relevant statistical quantities. The stiffness of a chain can be characterized by the characteristic ratio C_∞, the persistence length l_p, or the Kuhn length l_K of a chain. The characteristic ratio is defined as

$$C_n = \frac{\langle |\mathbf{r}_n|^2 \rangle}{n l_b^2} \tag{1}$$

with the asymptotic denoted as C_∞. Here $|\mathbf{r}_n|$ is the distance between two segments separated by n bonds, and l_b is the bond length.[28] The average is taken over all possible internal segment separations. A property closely related to C_n for describing the extent of the polymer, but which has the additional benefit of not depending on the choice of the (virtual) bond length, is $\langle |\mathbf{r}_n|^2 \rangle / M_n$, with M_n the molecular weight of n segments.

The persistence length l_p can be defined as the integral of a bond correlation function.[29] In the limit of infinitely long chains the persistence length is related to the characteristic ratio of the chain as $l_p = \frac{1}{2}(C_\infty + 1) l_b$.[28]

Another way to determine the stiffness of the chain is to measure the Kuhn length[30,29]

$$l_K = \lim_{n \to \infty} \left(\frac{\langle |\mathbf{r}_n|^2 \rangle}{r_{n,\max}} \right) \tag{2}$$

where $r_{n,\max}$ is the length of the chain in its maximally extended form. The Kuhn length can be interpreted as the bond length of an equivalent freely jointed chain, which has the same maximal extension $r_{n,\max}$ and the same root-mean-square (rms) end-to-end distance $\langle |\mathbf{r}_n(\varepsilon_{\mathrm{eng}})|^2 \rangle^{1/2}$ as the real chain in the limit of $n \to \infty$.[29,28]

To be able to compare with experimental results, the asymptotic C_∞ will be determined. Due to the relatively short chain length an extrapolation method should be used. To do so, two different fits will be used to describe the simulation results. The first one is

$$C_n = C_\infty (1 - \alpha' n^{-1/2}) \tag{3}$$

with α' a fit parameter. This is motivated by the recent simulation and theoretical result of Wittmer et al.[31] (theoretically demonstrated earlier by ref 32), where they show that due to long-range interactions in dense polymer systems the first-order correction to the ideal-chain limit is of $\mathcal{O}(n^{-1/2})$ in the melt.

The lowest-order correction from C_∞ for models of chains without excluded volume such as a chain with fixed bond angles and independent bond-rotational potentials[28] is $\mathcal{O}(n^{-1})$. The second fit-function we apply is therefore

$$C_n = C_\infty (1 - \alpha/n) \tag{4}$$

Although this result is not strictly valid in the melt, it is commonly used in other studies, such as ref 33. Results for both polymers are shown in appendix B.

Also in the determination of the Kuhn length deviations occur for relatively short chains when using the definition of l_K, eq 2.[28] An alternative we will use is to map the internal distances on the prediction for the worm-like chain (WLC), also known as the Porod−Kratky chain.[28,30,34] The mean square end-to-end distance for the Porod−Kratky chain with contour length L_c and stiffness length l_s is[28,30,34]

$$\langle |\mathbf{r}(L_c)|^2 \rangle = l_s \left(L_c + \frac{l_s}{2} \left(\exp\left(-\frac{2L_c}{l_s} \right) - 1 \right) \right) \tag{5}$$

In the limit of a very large contour length, $L_c/l_s \gg 1$, this equation reduces to $\langle |\mathbf{r}(L_c)|^2 \rangle = l_s L_c (1 + \mathcal{O}(l_s/L_c))$. In combination with eq 2 and $L_c = r_{n,max}$ it follows that $l_s = l_K$. In addition, the relation $l_p = l_s/2$ holds for the WLC.[28] The reason why we prefer to use the stiffness length over the Kuhn length is that we use it as a fitting parameter to describe deformed chains. In principle, eq 5 would change if a melt of chains is considered instead of an ideal worm-like chain, just as the extrapolation formula for the characteristic ratio changes from eq 4 to eq 3. This is, however, beyond the scope of the present study. Upon calculating the Kuhn length, the maximal extension for each polymer needs to be determined - these results are presented in appendix A. The Kuhn lengths of both polymers are given in appendix B.3.

4. Deformation and strain hardening

During constant-velocity uniaxial-stress extension simulations of PS and PC at $T = 300$ K the von Mises equivalent true stress[35]

$$\sigma = \sqrt{\frac{1}{2}(\sigma_x - \sigma_y)^2 + \frac{1}{2}(\sigma_y - \sigma_z)^2 + \frac{1}{2}(\sigma_z - \sigma_x)^2 + 3\sigma_{xy}^2 + 3\sigma_{yz}^2 + 3\sigma_{zx}^2} \tag{6}$$

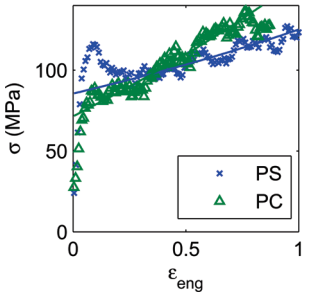

Figure 2. The von Mises equivalent true stress σ vs strain ε_{eng} for PS and PC. Solid lines are fits to eq 7. Fit range is $\varepsilon_{eng}=0.3-0.8$. Note that the strain-hardening modulus G_h for PC (24 MPa) is about twice that of PS (11 MPa), while their extrapolated offset yield values σ_Y are about the same (PS, 86 MPa; PC, 72 MPa).

is measured as a function of engineering strain

$$\varepsilon_{eng} = L_{||}(t_2)/L_{||}(t_0) - 1$$

(with t_0 the start time of deformation and t_2 the strained state; t_1 will be used for the initial strained state as will be explained later on). The result is shown in Figure 2 and is fitted by the Gaussian-based stress−strain relation

$$\sigma = \sigma_Y + G_h(\lambda^2 - \lambda^{-1}) \tag{7}$$

with the draw ratio $\lambda = 1 + \varepsilon_{eng}$. Here the two fit parameters G_h and σ_Y are the strain-hardening modulus and the offset yield value, respectively.

The so-determined strain-hardening modulus of PC is 24 MPa, about twice the PS value, 11 MPa, while the offset yield values are similar (PC: 72 MPa; PS: 86 MPa). They comply with our previous simulation results under slightly different conditions.[21] Experimental strain-hardening moduli are relatively close to the present results, $G_h=9-13$ MPa for polystyrene[5,24,36] and $G_h=23-29$ MPa for polycarbonate;[13,24,37] see also Table 1. As discussed in more detail before,[16,21] we can conclude that there exist a good agreement with experimental results, despite the obvious (counteracting) differences in deformation and cooling rates. Reasons for it may be the limited dependence of the strain hardening modulus on both rates. In case of PC it is experimentally observed[38] that the slope of the postyield stress−strain curve hardly changes, when the strain rate changes by more than 6 orders of magnitude. By means of MD simulations of PS[16] we observed that the only significant change upon changing the cooling rate by 1 order of magnitude occurred near the yielding regime - the post yield behavior did not seem to be affected.

What is the reason for the high strain-hardening modulus of polycarbonate over polystyrene and what causes strain hardening? That is the focus of the current study. The entanglement picture from rubber-elasticity theory predicts that the strain-hardening modulus equals $G_h = \rho k_B T/M_e$.[39] Here ρ is the mass density, and M_e is the mean molecular mass of the chain segments between effective entanglement points. This formula gives for polystyrene an estimation which is smaller by a factor of about 100 compared to experimental results.[4,5] It only implies that the strain-hardening modulus of PS is lower than that of PC. This is primarily because the molecular weight between effective entanglements in polystyrene is higher than in polycarbonate (PS, $T=$ 490 K, $M_e=18$ kDa; PC, $T=298$ K, $M_e=1.6$ kDa[20]). Here we want to take a different route in shedding more light on the difference in the strain-hardening moduli and look at nonaffine responses instead of entanglement effects.

5. The Role of Nonaffinity

5.1. Principle of Nonaffine Displacements. If a macroscopic sample is stretched in one direction (||) by, e.g., 100%, the distance between the two ends of the sample is doubled. If the stretching occurs purely affinely, then this is also valid for every two points on the stretching axis. At a microscopic level this affine response will break down due to particle−particle interactions such as connectivity and excluded-volume interactions. For example, it is highly improbable that a stiff covalent bond will be doubled in size. A more likely scenario is that the covalent bond retains its length and that particles tend to slip or slide along each other. Slippage causes friction and hence energy dissipation. One of the causes of friction is that Lennard-Jones bonds are broken and reformed. Another source is that conformational transitions occur. As long as the sample deforms approximately homogeneously, the deviation of each particle trajectory from the affine response results in a redistribution of the LJ bonds and in conformational transitions. Both frictions have, in general, a different weight in the nonaffine response. Although conformational transitions play an important role,[23,40] they are definitely not the sole friction effect causing strain hardening: in bead−spring models there are no conformational transitions yet strain hardening is still observed.[17] We therefore discard the different weight in the nonaffinity in the present study. In a subsequent study we may study these weights into more detail. To recapitulate, the average deviation from affinity is a measure for these frictions, so in turn a rough estimate of the dissipated energy, implying a measure of the plastic response and hence experienced stress of the material. In ref 41, it was demonstrated that nonaffine displacements are directly correlated to the experienced stress in a simple glass, thereby confirming this reasoning.

The assumption of homogeneous deformation can be made if no localization takes place. In our simulation method we are capable of applying an affine rescaling deformation (with a nonaffine response), so that localization is tempered and it is possible to measure the intrinsic stress−strain relation. At large strains localization does happen, because of fracture. Nevertheless, the first fractured sample for the studied polystyrene glasses occurs solely for strains larger than $\varepsilon_{eng}=0.8$. Also for polycarbonate large cavities start to form only after this strain value. Therefore, we assume that the deformation is approximately homogeneous until $\varepsilon_{eng}=0.8$.

5.2. Calculation of Nonaffine Displacements. In view of the suggested important connection between the plastic stress and the nonaffine displacement, we will calculate the latter. We adopt the definition being studied in our previous work[21] and other simulations of nonpolymeric systems.[41] Results of a different definition of the nonaffine displacement also exist,[17] but that definition has the strange effect that that nonaffine displacement can show an increase in nonaffinity while there is no nonaffine displacement going on.[42] Therefore we prefer the current definition. Basically, the local convective velocity arising from the global stretch is subtracted from the particle displacements. The subtraction is carried out for all three axes, as the perpendicular directions ($\perp_1$ and $\perp_2$) are also affected by the deformation. The component along one axis is denoted by μ, with $\mu = x, y, z$. Upon fixing the origin, the convective velocity at a certain position r^μ at time t is (without applying the Einstein summation convention)

$$v^\mu_{conv}(t) = \frac{r^\mu(t)}{L^\mu(t)}\left(\frac{L^\mu(t+\Delta t) - L^\mu(t)}{\Delta t}\right) \tag{8}$$

in the limit of $\Delta t \to 0$. Here $L^\mu(t)$ is the time-dependent length of the box along one axis represented by μ. The affine part is removed by constructing a "corrected" particle trajectory

Table 1. Strain Hardening Moduli of Present Simulation Results and Literature Experiments

property	polymer	this work	condition	experiments	condition	refs
G_h (MPa)	PS	11	ext	9, 11, 13	compr[a]	5, 24, 36
	PC	24	ext	23, 26, 29	ext,[b] compr and ext,[c] compr[d]	13, 24, 37

[a] $\dot{\varepsilon}_{true} = -10^{-3}$, -10^{-3} and -10^{-2} s^{-1} respectively. [b] $\dot{\varepsilon}_{true} = 10^{-2}$ s^{-1}. [c] For both $|\dot{\varepsilon}_{true}| = 10^{-2}$ s^{-1}. [d] $\dot{\varepsilon}_{true} = -10^{-3}$ s^{-1}.

$\mathbf{r}_c(t)$ from the original one $\mathbf{r}_o(t)$ by subtracting the convective velocity $\boldsymbol{v}_{conv}(t)$ at the position $\boldsymbol{r}_o(t)$

$$\mathbf{r}_c(t+\Delta t) - \mathbf{r}_c(t) = \mathbf{r}_o(t+\Delta t) - \mathbf{r}_o(t) - \mathbf{v}_{conv}(t)\Delta t \qquad (9)$$

For the corrected trajectories we will only analyze differences in positions of the same particle, hence the initial position $\boldsymbol{r}_c(t_0)$ is irrelevant. The calculation of the nonaffine part of the particle's trajectory is carried out on the stored trajectory file, in which snapshots are saved every $\Delta t = 8$ ps. In principle eq 9 is only valid for $\Delta t \to 0$. Nevertheless, artificially increasing the time step between frames by only processing the odd frames does not lead to any significant difference in the final acquired corrected trajectory. Note that the result of this method, apart from a constant term, is independent of the choice of the origin t_0. Note also that in case of a constant-volume simulation without any deformation the convective velocity equals zero making the corrected particle trajectory equal to the original particle trajectory. In this situation the mean-square nonaffine displacement $\langle \Delta \mathbf{r}_c(t)^2 \rangle = \langle (\mathbf{r}_c(t_0+t) - \mathbf{r}_c(t_0))^2 \rangle$ obviously equals the normal mean-square displacement $\langle \Delta \mathbf{r}_o(t)^2 \rangle$. For simplicity we will drop the "c" when no confusion arises.

5.3. Isotropic vs Deformed Nonaffine Bead Displacements. In this section, we study the nonaffine bead displacement between two states. For the deformed samples one state will be the unstrained state

$$\langle \Delta \mathbf{r}(\varepsilon_{eng,20})^2 \rangle^{1/2} = \langle (\mathbf{r}_c(\varepsilon_{eng}) - \mathbf{r}_c(0))^2 \rangle^{1/2} \qquad (10)$$

Here $\varepsilon_{eng,20} = \varepsilon_{eng,2} - \varepsilon_{eng,0} = \varepsilon_{eng} - 0 = \varepsilon_{eng}$. The subscript 0 is included explicitly to indicate that $\langle \Delta \mathbf{r}(\varepsilon_{eng,20})^2 \rangle^{1/2}$ also depends on the unstrained state. Previous studies[16,17,21] calculated this nonaffine displacement as well (or a different definition, see section 5.2) to study the strain-hardening behavior of a polymer model, albeit no distinction was made between different groups of atoms. It will be shown that in the chemically detailed model the behavior of various groups of atoms differs substantially and that this brings in new information that cannot be addressed by the bead−spring model.

The nonaffine displacement $\langle \Delta \mathbf{r}(\varepsilon_{eng,20})^2 \rangle^{1/2}$ for both polymers during uniaxial extension is shown in Figure 3. Also shown in the same figure is the root-mean-square translational displace-ment for the undeformed case at the same temperature (denoted by "iso"), by plotting the data at equal time separation $t_2 - t_0 = t_{20} = \tau_{def}\varepsilon_{eng,20}$. Here τ_{def} is the time it takes to deform the material to a 100% strain increment.

Notice that after initial yield the deformed samples have a large increase in nonaffine displacement as compared to the isotropic case. The mean-square displacement for the isotropic case hardly rises in this region (bounded to about 1 Å for PS and 2−3 Å for PC); a consequence of the caging of the particles deep in the glassy state (studied in more detail in our previous studies, refs 43 and 16). The increase of nonaffine displacement in the deformed case implies that the particles have moved outside their original cages.

When comparing polycarbonate to polystyrene the following is visible. Up to about 40% deformation the nonaffine displacement of all (united) atoms of PS is about equal to that of PC. Afterward, the nonaffine displacement of PS diminishes as compared to PC. Also apparent is the difference between the movement of all atoms and the movement of only a subset of atoms (the less mobile backbone atoms). For polycarbonate the difference is small; the average displacement of all atoms does not differ much from the average nonaffine displacement of only the $C_{C=O}$ and the CT atoms (the two least mobile backbone atoms in the isotropic state, with $C_{C=O}$ in the carbonate group and CT the middle carbon of the propane part of the monomer, see Figure 1b). For polystyrene, however, a large difference is present between the movement of all atoms and that of the subset (the backbone united atoms CH, CH_2, and the chain ends CH_3, see Figure 1a).

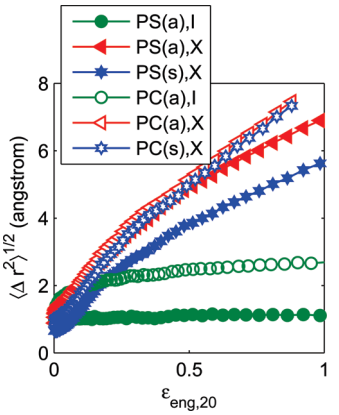

Figure 3. Root-mean-square nonaffine united-atom displacement as a function of strain for polystyrene (filled markers) and polycarbonate (open markers) under the influence of active deformation (indicated by "X"). For comparison, the isotropic (indicated by "I") root-mean-square displacement at equal time separation ($t_2 - t_0 = \tau_{def}\varepsilon_{eng,20}$) is also shown. A distinction is made between all united atoms (a) and only the least mobile subset of them (s). See text for details.

An interpretation of this is that the side-group phenyl rings in polystyrene dominate the generation of initial plastic flow. However, these side-group phenyl rings can relatively easily turn in the plane perpendicular to the backbone vector pointing from one monomer to its neighbor, without disturbing the conformation of the backbone too much; therefore the phenyl rings will not drag along the backbone for all nonaffine displacements. This could also explain the relatively large difference between the nonaffine displacement of all atoms and the nonaffine displacement of the backbone in PS. We will see later that it is just the backbone that causes the strain-hardening effect. As the contribution of the backbone to the total nonaffine displacement is only minor in PS, the resulting overall plasticity is less affected by the backbone. In polycarbonate, in contrast, no real side groups are present, and the available phenyl rings are within the backbone; therefore any motion of those rings (apart from rotation around their own axes) will lead to backbone motion and any increase in the backbone plasticity will also lead to a large increase in the overall plasticity.

5.4. Rate of Nonaffine Bead Displacements. The nonaffine displacement as shown in Figure 3 and discussed in the previous section is calculated by comparing a sample at a strained state with respect to the state at zero strain. This nonaffine displacement increases with increasing strain. However, also for a nonpolymeric glassy material this is what one would expect, despite the absence of any polymeric

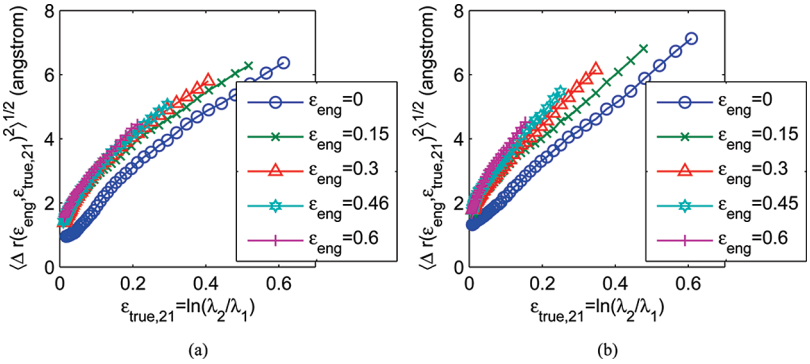

Figure 4. The rms nonaffine displacement as a function of relative extension (true-strain difference $\varepsilon_{true,21}$) for various values of the origin ε_{eng} for (a) PS and (b) PC. At a later stage more nonaffine displacement is necessary to deform the material. This effect is stronger for polycarbonate, as can be seen by the spread in the curves at large $\varepsilon_{true,21}$.

strain hardening. See, e.g., ref 41, where the nonaffine displacement for an atomic LJ glass increases in a diffusion-like matter under the influence of shear. Yet another cause is that of thermal motion. As the deformation is at a constant engineering strain rate, strain differences correspond to time differences. Nonaffine displacements can therefore also be regarded as being a function of time. In the undeformed, isotropic case, the convective velocity is zero so that the nonaffine rms displacement is equal to the normal rms displacement. And this normal rms displacement simply increases due to thermally activated motion. So even for the undeformed, isotropic case the root-mean-square nonaffine displacement is increasing with time.

We therefore need a different measure to see evidence for a connection between the rate of energy dissipation and nonaffine displacement. We will look at the plasticity rate, i.e., the *rate* of nonaffine displacement. As will be discussed later this will not increase for particles in a simple glass undergoing a steady-steate deformation and for diffusing particles in equilibrium and therefore isolates the polymeric effect. Previous MD studies on strain hardening effects in polymer glasses as mentioned in the previous section have only shown results of nonaffine displacements and not of the rate of nonaffine displacements.

The practical implementation of detecting the rate of nonaffine displacement as a function of strain is to compare the nonaffine displacement at different origins, in which each origin corresponds to a different strained state "1" rather than only the undeformed state "0". The nonaffine displacement is then a function of both the origin "1" (denoted by $\varepsilon_{eng}=\lambda_1-1$) and the relative separation "2−1" (denoted by $\varepsilon_{true,21} = \varepsilon_{true,2} - \varepsilon_{true,1} = \ln(\lambda_2/\lambda_1)$)

$$\langle \Delta \mathbf{r}(\varepsilon_{eng}, \varepsilon_{true,21})^2 \rangle^{1/2} = \langle (\mathbf{r}_c(\lambda_2) - \mathbf{r}_c(\lambda_1))^2 \rangle^{1/2} \qquad (11)$$

The nonaffine displacement is taken as a function of the relative increase in strain

$$\varepsilon_{true,21} = \ln\left(\frac{L_{||}(t_2)}{L_{||}(t_1)}\right)$$

instead of a function of the difference in engineering strain

$$\varepsilon_{eng,21} = \frac{L_{||}(t_2) - L_{||}(t_1)}{L_{||}(t_0)}$$

to compare relative extensions instead of absolute ones at an equal footing. Obviously, the latter is not invariant under a shift in t_0.

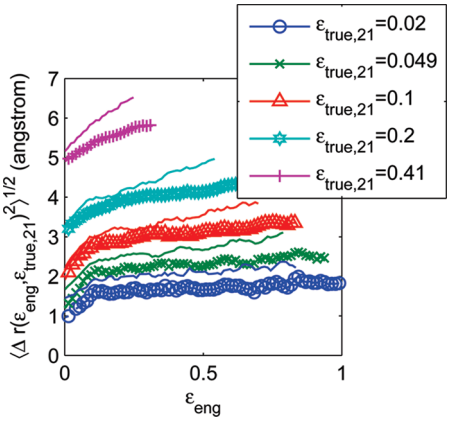

Figure 5. Measure for the rate of nonaffine displacement as a function of strain ε_{eng} at various separation strains $\varepsilon_{true,21}$ for PS (markers) and polycarbonate (solid lines). Note that it is increasing with strain and is always higher for PC.

Equation 11 also corresponds to looking at the nonaffine MSD for various time origins, because, again, differences in strain correspond to differences in time. In an equilibrium isotropic situation the normal rms displacement (and hence the rms nonaffine displacement) would be independent of the time origin, so that by looking at different origins any possible increase would be solely due to the increase in plasticity with strain, and not a result of stationary plasticity or equilibrium thermal motion. In a glass, there is an aging effect and the rms nonaffine displacement does also depend on the time origin, but the simulation results show that for PS no systematic increase with time is present and for PC there is even a decrease in the nonaffine displacement with longer aging time for a constant time interval (which is to be expected[16]).

The rms nonaffine displacement $\langle \Delta \mathbf{r}(\varepsilon_{eng},\varepsilon_{true,21})^2 \rangle^{1/2}$ is a two-dimensional function. We therefore plot it both as a function of the relative extension $\varepsilon_{true,21}$ for various values of the origin ε_{eng} (Figure 4) and as a function of ε_{eng} for various values of $\varepsilon_{true,21}$ (Figure 5, which is a measure for the change in the rate of nonaffine displacement as a function of ε_{eng}). The motive is that some effects turn out to be more clearly visible in one of the two representations. In plotting the rms nonaffine displacement as a function of ε_{eng} for various values of $\varepsilon_{true,21}$ one point should be addressed. The saved trajectory file has a finite time step between frames, so that there is not always a pair of two frames available for a given value of $\varepsilon_{true,21}$. As the first frame is already determined by ε_{eng}, the second frame is chosen as that which renders the closest value of the required

$\varepsilon_{true,21}$. If the $\varepsilon_{true,21}$ from this pair of frames deviates by more than 5% from the requested $\varepsilon_{true,21}$ the point is discarded.

A few observations are visible when looking at the nonaffine displacement as a function of $\varepsilon_{true,21}$ and ε_{eng} for both polymers in Figure 4 and Figure 5. We first focus on the initial yield regime. It clearly has a large effect on the increase in nonaffine displacement. The nonaffine displacement at small relative strains $\varepsilon_{true,21}$ increases substantially as a function of ε_{eng} during the first few percents of deformation, i.e., up to the initial yield point. For ε_{eng} beyond the initial yield region the relative increase is much lower. Also, the increase in the nonaffine displacement as a function of $\varepsilon_{true,21}$ for values of $\varepsilon_{true,21}$ smaller than about 0.05 is steeper for larger ε_{eng}.

These observations near yield can be understood by the following picture. Straining the unstrained sample is initially mostly elastic. This is supported by the simulation result of our previous study[16] that most of the initial applied work is converted into internal energy. The elastic response causes only a small deviation from an ideal pure affine response as no significant structural rearrangements occur. After initial yielding rearrangements do occur and the mobility of atoms is at an enhanced level, the fluctuations around the ideal affine trajectory are in this case larger than in the undeformed case. As the average rms difference between two very fluctuating signals (i.e., between two strained samples) is larger than the average rms difference between a very fluctuating signal and a less fluctuating signal (i.e., between the unstrained and the strained sample), the nonaffine displacement for small values of $\varepsilon_{true,21}$ is expected to be larger after yield.

Let us now focus on the second regime, that of strain-hardening. Here the first and most important observation is that at larger values of ε_{eng} more nonaffine displacement is indeed needed to establish the same relative extension. Because one of the main aims of the current study is to explain this effect, we dive deeper in the underlying reason in the next sections, 5.5 and 5.6. To illustrate the effect more clearly, consider the data of polystyrene in Figure 4. In order to stretch the sample by 22% ($\ln(\lambda_2/\lambda_1) = 0.2$) about 3.2 Å of nonaffine displacement per united atom is necessary if the initial state is the unstrained one. However, if the initial state equals $\varepsilon_{eng} = 0.15$, then about 3.8 Å of nonaffine displacement is needed to increase the sample in the extension direction by the same relative amount. This value of nonaffine displacement keeps on increasing in the strain-hardening region. The particles are moving more nonaffinely at larger strains, implying that larger detours or deviations around the affine response are unavoidable at larger strains. This relative increase in nonaffine displacement with increasing strain is larger for polycarbonate than for polystyrene, which can be clearly seen by the larger slope for PC of the curves in Figure 5 (note that it is much clearer than when one only studies the evolution of the nonaffine displacement, as depicted in Figure 3). The polymer structure apparently imposes the magnitude of detours from affinity.

Another observation in the strain-hardening regime is that the slope of the curves in Figure 5 increases with $\varepsilon_{true,21}$. Apart from the absolute value (larger values of $\varepsilon_{true,21}$ simply means a larger separation between the two strained states), the slope of the curve normalized by the rms nonaffine displacement at a fixed value of ε_{eng} is also increasing with $\varepsilon_{true,21}$ (not shown). The origin might be the influence of thermal motion. Small strain differences correspond to small time scales. For these small time scales nonaffine displacements in the stressed state are comparable to the normal thermally activated displacements in the undeformed case and the pure nonaffine increase is somewhat overshadowed by thermal motion. At larger strain differences $\varepsilon_{true,21}$ the relative contribution of the thermal motion is smaller, resulting in a more pure nonaffine increase. A similar situation is present when one considers a vector in space. If one component of the vector is increasing and other components are constant and nonzero, the relative increase in the length of that vector is less than the increase in the component. If, on the other hand, other components are negligible, the relative increase in the length of the vector is equal to that of the component. Therefore, one expects that for larger strain differences of $\varepsilon_{true,21}$, in which the relative contribution of the thermal motion is smaller, the resulting slope is higher.

It turns out that there is even a quantitative agreement between the measure for the rate of nonaffine displacement and the amount of strain hardening. We apply a Gaussian fit similar to eq 7 for the stress but now for the rate of nonaffine MSD $f = \langle \Delta \boldsymbol{r}(\varepsilon_{eng},\varepsilon_{true,21})^2 \rangle$ as a function of $\lambda^2 - \lambda^{-1}$ (with $\lambda = 1 + \varepsilon_{eng}$ and only taking into account values larger than $\varepsilon_{eng} = 0.3$) for $\varepsilon_{true,21} = 0.05$. The resulting fit equation is for PS $f = 4.5$ Å$^2 + 0.61$ Å$^2(\lambda^2 - \lambda^{-1})$ and for PC $f = 4.8$ Å$^2 + 1.7$ Å$^2(\lambda^2 - \lambda^{-1})$. Observe that the ratio of the slope to the offset is very close to the same ratio of the strain hardening modulus to the yield modulus G_h/σ_Y, eq 7. The former is for PS 0.13 and for PC 0.35, while the latter is for PS 0.12 and for PC 0.33, thereby confirming the link between the slope of the rate of the squared nonaffine displacement and the strain hardening modulus.

The current results regarding the increase in the rate of nonaffine displacement for the two polymers in the strain-hardening regime are in accordance with two previous studies on polymers where also an increase in a different mobility-related rate is observed during deformation. In a polyethylene-like model polymer[23,40] a steady increase in the torsion transition rate can be seen in the postyield regime (the strain-hardening region). A study on a polymer bead−spring model at zero temperature[9,10] revealed that the rate of changes in LJ binding is also increasing in the strain-hardening regime and, moreover, that it is directly correlated with the dissipative stress at zero temperature. These observations suggest that such rate increase during deformation is quite universal in glasses of linear polymers.

5.5. Nonaffine Deformation of Polymer-Chain Shape. What is causing the increase in the rate of nonaffine displacement for the polymer glass? One reason for the nonaffine displacement is that covalent bonds prevent the separation of the bonded particles. If particles would displace affinely, then the equilibrium value of this chemical bond would be excessively disturbed, accompanied with large forces. This will be circumvented, so that the bond vector will not change affinely with the deformation and hence the same for the particles forming that bond. At much larger length scales such as the end-to-end distance an affine response is possible; the internal conformation of a long chain can be adjusted, while still obeying to the equilibrium length of the covalent bond (the effective spring constant associated with the end-to-end distance is much less stiff). Moreover, due to the glassy state the relaxation time of spontaneous rearrangements at the scale of the whole chain greatly exceeds experimental and simulation time scales (as mentioned in section 1) so that the end-to-end distance cannot adjust back toward the equilibrium value by means of spontaneous relaxations. Hence, the end-to-end distance will follow the imposed deformation much more affinely. We therefore expect an increase in the affine response, if we probe larger length scales. By means of measuring the chain structure factor by means of neutron scattering

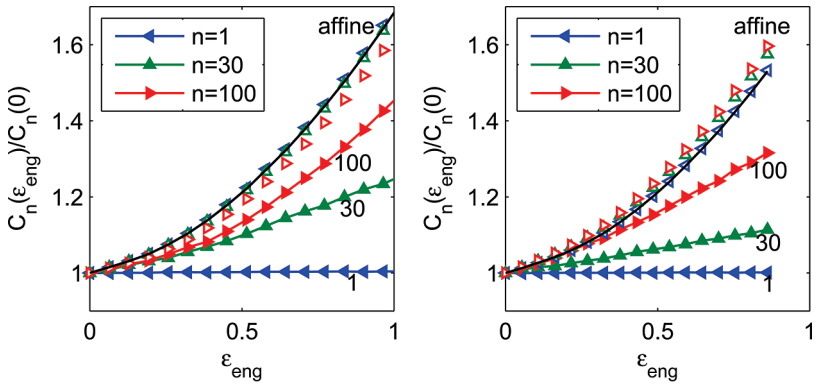

Figure 6. Normalized characteristic ratio $C'_n(\varepsilon_{eng}) = C_n(\varepsilon_{eng})/C_n(0)$ as a function of strain for (a) PS and (b) PC. Filled symbols with solid lines are simulation results, while the open (higher) symbols are results as if the same sample would deform in an affine way. The top solid curve (in black) is the affine approximation, eq 14.

of a polymer glass (PMMA, ref 44) it is indeed observed that larger length scales behave more affinely. In simulations, nevertheless, we can directly probe the internal distances of the polymer chain.

We will use the following method to see the deviations from affinity in a quantitative way. In section 3 the statistical quantities to measure the internal distances are introduced. We want to compare the deformed internal distances both to the undeformed ones (the limit if the distances do not change at all from the undeformed state) and to the internal distances if their response with deformation would be purely affine (the ideal affine limit). This is realized by examining the evolution of the characteristic ratio, eq 1, during deformation normalized by the isotropic case

$$C'_n(\varepsilon_{eng}) = C_n(\varepsilon_{eng})/C_n(0) = \langle|\mathbf{r}_n(\varepsilon_{eng})|^2\rangle/\langle|\mathbf{r}_n(0)|^2\rangle \quad (12)$$

Here the dependence of C'_n on the unstrained state is not shown in the argument for the sake of a shorter notation. A similar quantity was studied in ref 10, but there the focus was on entanglement effects. Here we want to study it without taking this into mind.

To see the deviations of the stretching at various scales from the affine response, this affine response is also calculated. We use two different methods. The first method is to affinely transform the coordinates of all particles at $\varepsilon_{eng} = 0$ according to the relative change in box sizes, meaning that for the x-components of the coordinates

$$x_{n,aff}(\varepsilon_{eng}) = \lambda_x x_n(0) \quad (13)$$

with $\lambda_x = L_x(t)/L_x(0)$. The coordinates in the direction of the two other axes (y and z) are rescaled likewise. Afterward, the characteristic ratio of the affinely transformed coordinates is calculated. The second method is to assume that the initial sample is isotropic in the sense that $\frac{1}{3}\langle|\mathbf{r}_n|^2\rangle = \langle|x_n|^2\rangle = \langle|y_n|^2\rangle = \langle|z_n|^2\rangle$. The affine response for the squared intrachain length scales including this isotropy condition equals

$$\langle|\mathbf{r}_{n,aff}(\varepsilon_{eng})|^2\rangle = \frac{1}{3}(\lambda_x{}^2+\lambda_y{}^2+\lambda_z{}^2)\langle|\mathbf{r}_n(0)|^2\rangle \quad (14)$$

Hence $C'_{aff}(\varepsilon_{eng}) = \frac{1}{3}(\lambda_x{}^2+\lambda_y{}^2+\lambda_z{}^2)$ which is independent of n.

Results for the normalized characteristic ratio of polystyrene and polycarbonate are plotted as a function of ε_{eng} in Figure 6, closed symbols. The ideal, affine responses are also included. Open symbols are the result of calculating the affine response by the first method. The results of the second method, assuming that the sample would be isotropic before deformation, are shown as solid lines (upper curves).

Note that the two ways of calculating the affine response are close to each other, meaning that the samples can be regarded as being isotropic (in this sense). For large n less data points are available (poorer statistics) and the two methods deviate more from each other.

The following observations are apparent from Figure 6. As is expected, C_1 and hence C'_1 are almost unchanged with increasing extension, for polystyrene as well as for polycarbonate. This is due to the very rigid covalent bond. For somewhat larger separations the internal distance is able to increase, although the response is subaffine, see, e.g., the evolution of C'_{30}. For even larger separations an almost affine response is present, see, e.g., C'_{100}. This internal distance responds affinely up to about 15% for both polystyrene and polycarbonate. For larger strains the relative deviation from affinity for even C'_{100} becomes larger.

We can conclude that upon deforming further, larger and larger segments move in a nonaffine way for the two chemically detailed polymer models. This is in accordance with the results of the bead−spring model[10] (and therefore refutes the hypothesis that our chains would not deform nonaffinely as mentioned in ref 17) and with what was found in section 5.4 for the increase in nonaffine displacement of beads upon straining. As discussed earlier, the nonaffine bead displacement at a fixed relative strain is also at a higher level at larger strain origins. It is therefore plausible that the increase in the relative nonaffine bead displacement at larger strains is caused by the fact that at larger strains larger chain segments move nonaffinely.

So a connection can be made between strain hardening, nonaffine displacement of particles, and nonaffine stretching of intrachain distances. If larger chain parts reshape nonaffinely, then the accompanying beads of the chain parts move more nonaffinely as well. A larger force is needed to move particles more nonaffinely, so that this leads to an increase in the stress. So strain hardening is caused by the more nonaffine reshaping of the internal distances of a chain.

Let us now focus on the differences between PS and PC. For both polymers larger segments move nonaffinely at larger inner length scales. The difference is the magnitude of the effect. This is exemplified by the stretch of the internal distance corresponding to $n = 30$ at $\varepsilon_{eng} = 0.5$. For polycarbonate $C'_{30}(0.5)$ is almost 30% of the affine value, $C'_{aff}(0.5)$, see Figure 6b. For polystyrene the response is

more affine for $n = 30$; in this case 50% of the affine value is reached at $\varepsilon_{eng} = 0.5$, Figure 6a.

One could argue that the deviation from affine response should be compared at equal contour lengths instead of equal number of backbone bonds. Nevertheless, this does not change the conclusion if we define the contour length as the total length via covalent backbone bonds. This is justified by the fact that the rms backbone bond length $\langle l_{bb,i}^2\rangle^{1/2}$ is in fact very similar for both polymers. For PS $\langle l_{bb,i}^2\rangle^{1/2} = 1.53$ Å. To determine the backbone bonds for PC we take one of the shortest pathways via covalent bonds from the start of one monomer to the start of the subsequent monomer. In this way we encounter $2l_{C_{c=o}-O}$, $2l_{O-C_+}$, $2l_{C_+-CH}$, $2l_{CH-CH}$, $2l_{CH-C}$ and $2l_{C-CT}$ (see Figure 1b), making $\langle l_{bb,i}^2\rangle^{1/2} = 1.42$ Å.[27] The difference between the PS and PC rms backbone bond lengths is thus less than 10%, so that also for equal contour lengths the nonaffine response is larger for PC.

This behavior of a more nonaffine chain-shape response for PC as opposed to PS can be connected to the previous finding regarding the root-mean-square nonaffine bead displacement. Also in terms of the bead displacements PC behaves more nonaffinely than PS: the nonaffine displacement at a certain value of $\varepsilon_{true,21}$ increases more with increasing strain for PC than for PS (compare Figure 4a with Figure 4b).

5.6. Effective Chain Stiffness during Deformation. So what would be the reason for the difference in increase in the nonaffine response of the inner chain dimensions between PS and PC? To answer this question we again take a closer look at the internal distances of the chain. As observed in the previous section covalent bonds will maintain their initial length (the bond will slip instead) and for very large scales the behavior is also evident: if the maximal extensibility of the chain is much higher than the draw ratio and the relaxation time exceeds the time scale of deformation (as is the case for the glassy state), the displacement at these scales will be approximately affine. For particles within a chain which are separated by several bonds the situation is within these two limits and depends on the maximal extensibility of the chain at that length scale. Previous simulation studies on polymer glasses[10] have only concentrated on the deviation of the chain shape with respect to the affine response and not with respect to the maximal extensibility. To understand the behavior of the intrachain distances during deformation it is crucial to also study this extensibility limit.

At the scale of the Kuhn length, eq 2, the chain cannot be extended any further and a nonaffine stretching of this length cannot be circumvented. The maximal (reasonable) extensibility at any internal distance n as a function of strain is the ratio of the end-to-end distance of the fully extended chain to the random-coil conformation of the chain

$$\lambda_{n,\max}(\varepsilon_{eng}) = \sqrt{C_{n,\max}/C_n(\varepsilon_{eng})} = \frac{r_{n,\max}}{\langle|\mathbf{r}_n(\varepsilon_{eng})|^2\rangle^{1/2}} \quad (15)$$

For the two simulated polymers the maximal draw ratio $\lambda_{n,\max}$ is plotted in Figure 7 as a function of the maximal extension $r_{n,\max}$ for a certain number of backbone bonds n and for various values of ε_{eng} (the method for determining the fully extended state of PS and PC is described in appendix A). If we do not use $r_{n,\max}$ for the horizontal axis, but the number of backbone atoms n, or the average backbone length times the number of backbone atoms $\langle l_{bb,i}^2\rangle^{1/2}n$, then Figure 7 hardly changes.

In Figure 7 we observe that an atactic PS chain is able to extend much more than a PC chain for a certain fixed

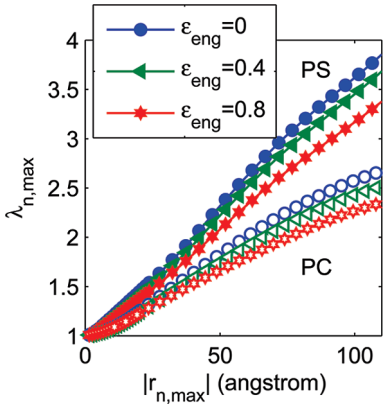

Figure 7. Simulation results of the maximal extensibility $\lambda_{n,\max}$ (eq 15) for PS (filled symbols) and PC (open symbols) as a function of the maximal extension $r_{n,\max}$ (approximately equal to the contour length) for different values of strain ε_{eng}.

distance along the chain, reminiscent of the observation that the Kuhn length of PS is much lower than that of PC. This implies that during a uniaxial-stress extension experiment, the polystyrene chain is able to move more affinely, as is illustrated in Figure 8.

Also noticeable in Figure 7 is that during deformation the maximal extensibility $\lambda_{n,\max}(\varepsilon_{eng})$ decreases for larger scales. More and more segments are moving nonaffinely upon straining, leading to an increase in the rate of nonaffine displacements. Due to the observed correlation of the latter with strain hardening in section 5.4, the latter leads to an increase in the rate of plastic events and causes the hardening in the stress upon straining. Obviously the decrease of the maximal extensibility is caused by the stretching of the chains. Can we understand in which way this extensibility, and accompanied with it the intrachain distances, change upon straining?

That can be easily determined by mapping the strained chain on an effective freely jointed chain (FJC) (or on an effective worm-like chain (WLC) if $L_c/l_s \gg 1$, eq 5, as the expression for the Kuhn length, eq 2, is the same in this limit). The large-scale internal-chain distances deform nearly affinely, in a way given by eq 14. The effective stiffness of the chain, however, increases, as can be concluded from the following discussion.

First we consider a chain C in a one-dimensional space. Let us denote the unperturbed, ideal chain by $C(0)$. If that chain would be stretched, so that the end points transform affinely by a factor $\lambda = 1 + \varepsilon_{eng}$ (but do not exceed the contour length L_c), then one can map the resulting deformed chain $C(\varepsilon_{eng})$ on an effective isotropic, undeformed freely jointed chain $C_{eff}(0)$ but with the same contour length and average end-to-end distance as the deformed chain $C(\varepsilon_{eng})$. This effective FJC $C_{eff}(0)$ has a Kuhn length which is different from the Kuhn length of the unperturbed one-dimensional chain prior to deformation $C(0)$, as the end-to-end distance of the effective chain $C_{eff}(0)$ is larger than the end-to-end distance of the unperturbed chain $C(0)$. We will now define the effective Kuhn length of the deformed chain $C(\varepsilon_{eng})$ as being equal to the Kuhn length of the effective chain $C_{eff}(0)$. To avoid any confusion with the intrinsic Kuhn length of the unperturbed chain $C(0)$, we will call the effective Kuhn length of a deformed chain $C(\varepsilon_{eng})$ the *effective stiffness length* $l_s(\varepsilon_{eng})$. Take $x(0)$ to be the end-to-end distance of the chain $C(0)$. Then $x_{aff}(\varepsilon_{eng}) = \lambda x(0)$ and hence the effective stiffness length during deformation equals $l_{s,aff}(\varepsilon_{eng}) = x_{aff}(\varepsilon_{eng})^2/L_c = \lambda^2 l_s(0)$. So upon stretching the chain, the

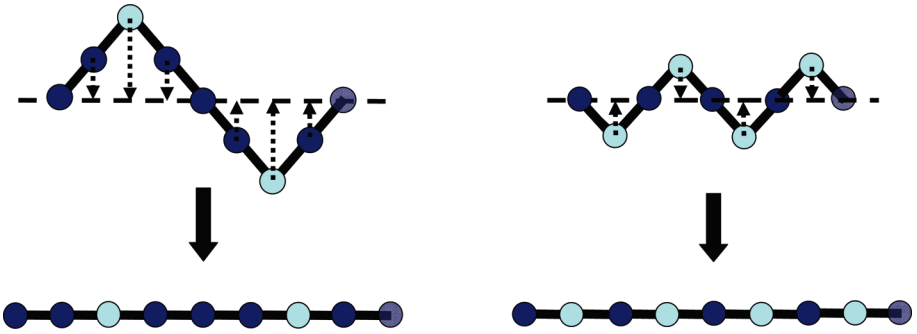

Figure 8. Illustration showing that a chain which has a larger Kuhn length (upper left chain, which has a pivoting point every fourth particle, indicated by the lighter particle) needs more nonaffine displacement to stretch further than a chain with a smaller Kuhn length (upper right chain, which has a pivoting point every second particle). The dotted arrows indicate the amount of vertical nonaffine displacement necessary for each particle in the two upper chains if the two end atoms of each chain are displaced from each other by the same amount in the horizontal direction, i.e., horizontal extension. Hence, the total vertical nonaffine displacement per particle of the stiffer chain on the left side is twice that of the more flexible chain on the right side.

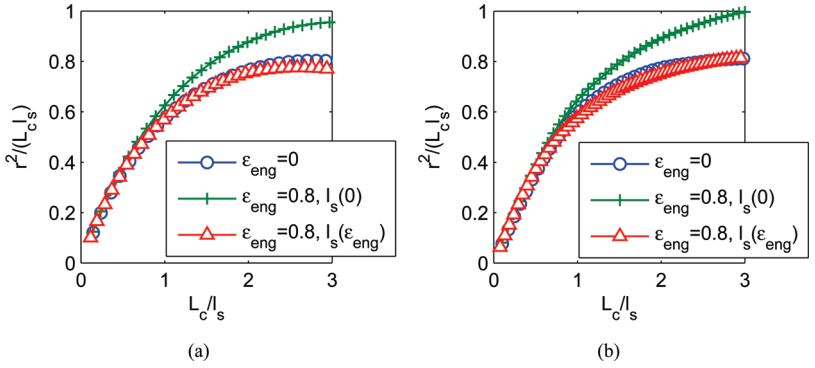

Figure 9. The normalized squared intrachain length $\langle|\mathbf{r}|^2\rangle/(L_c l_s)$ as a function of the normalized chain contour length L_c/l_s for (a) PS and (b) PC. When normalized by the effective stiffness length $l_s(\varepsilon_{eng})$ during deformation instead of the stiffness length of the unperturbed chain $l_s(0)$, the curve at a strained state turns out to be almost superimposable on the unstrained curve, demonstrating that the intrachain lengths can be accurately described by an increase in the effective stiffness length during deformation.

effective perturbed-chain stiffness length starts to deviate from the unperturbed-chain stiffness length—it increases.

The calculation in three dimensions is equivalent. A point to mention is that now the chain shape will deform in an anisotropic way. Therefore it is expected that the internal distances of the effective chain C_{eff} will deviate from the internal distances of the deformed chain. Nevertheless, we can still define an effective stiffness length of the deformed chain, by again equating the end-to-end distance and the contour length of the deformed chain with an effective nondeformed chain in the long-chain limit and taking the Kuhn length of that effective chain as the effective stiffness length of the deformed chain. If the end points of the deformed chain transform affinely, the effective stiffness length as a function of strain equals

$$l_{s,\,\mathrm{aff}}(\varepsilon_{\mathrm{eng}}) = l_s(0)\frac{1}{3}(\lambda_x{}^2+\lambda_y{}^2+\lambda_z{}^2) \qquad (16)$$

When assuming incompressibility, it is easy to see from eq 16 that the effective stiffness length increases during uniaxial extension. As the nonaffine particle displacements during deformation increase with increasing stiffness length it is natural to expect that the rate of nonaffine displacement of the backbone increases with strain in a way similar to the increase in effective stiffness length. This is illustrated in Figure 8.

Due to the limited chain length in our simulations we cannot determine the long-chain stiffness length l_s by using eq 2. Instead, we will use the worm-like chain expression, eq 5, for determining the effective stiffness length. However, the deformed chains are in generally anisotropic and therefore it is likely that the functional dependence of the intrachain distances would deviate from the renormalized ideal WLC result. A possible direction of improvement would be to replace the WLC model by a distribution of internal distances that has more parameters and that takes the anisotropy of the deformed chain explicitly into account. For example, this could be necessary to explain the Bauschinger effect in polymer glasses.

Nevertheless, on the basis of our simulation data, we can conclude that mapping the deformed chain back onto an isotropic WLC albeit with an increase in the effective stiffness length does suffice for describing the internal distances. This evidence is presented in Figure 9, where the normalized squared intrachain length scales $\langle|\boldsymbol{r}|^2\rangle/(L_c l_s)$ as a function of the normalized chain contour length L_c/l_s is displayed. If the normalization is carried out by using the stiffness length of the unperturbed chain the intrachain lengths increase with strain, as expected. If, on the other hand, we fit the deformed intrachain lengths as a function of contour length by the intrachain lengths according to the isotropic WLC model, eq 5, to determine the effective stiffness length and use this effective stiffness length to normalize the intrachain and the contour lengths, we see that the intrachain lengths do remain approximately invariant under the influence of deformation (both for PS and PC, see Figure 9). As with determining the characteristic ratio (see appendix B.1 and B.2), the fit for determining the effective stiffness length is confined to contour lengths smaller than 3 stiffness lengths, because the chains under consideration are not perfectly ideal for large scales (the decline in the characteristic ratio, Figure 10 and appendix B).

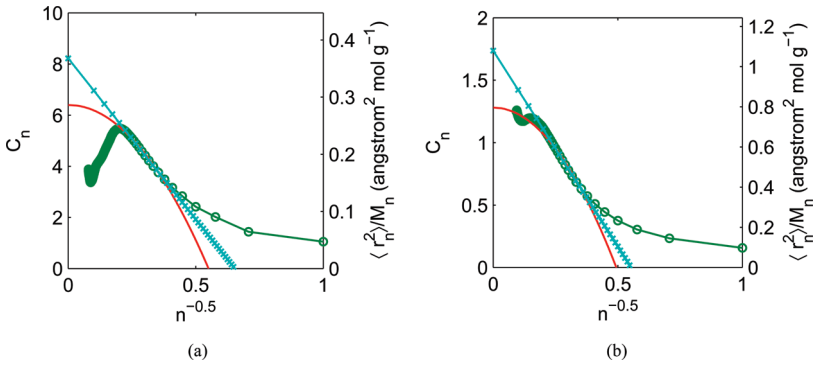

Figure 10. Characteristic ratio C_n at $T = 300$ K as a function of the inverse of the square root of the number of skeleton bonds for (a) PS and (b) PC. Circles indicate the simulation results, crosses fits by eq 3, and solid lines fits by eq 3. Melt-chain fit results are for PS, $C_\infty = 8.2$ and $\langle|\mathbf{r}|^2\rangle/M = 0.37$ Å^2 mol g^{-1}, and for PC, $C_\infty = 1.7$ (for $l_{b,PC} = 12.63$ Å) and $\langle|\mathbf{r}|^2\rangle/M = 1.1$ Å^2 mol g^{-1}. Ideal-chain fit results are for PS, $C_\infty = 6.4$ and $\langle|\mathbf{r}|^2\rangle/M = 0.29$ Å^2 mol g^{-1}; and for PC, $C_\infty = 1.3$ (again for $l_{b,PC} = 12.63$ Å) and $\langle|\mathbf{r}|^2\rangle/M = 0.80$ Å^2 mol g^{-1}.

To sum up, the effect of deformation on the intrachain distances can be interpreted simply as an increase in the effective stiffness length of an equivalent WLC. Again, in this analysis there is no need to consider the length scale at which entanglements start to play a role or other entanglement effects (except when the contour length between entanglements becomes stretched, to be discussed later on). Also, in contrast to this analysis, in the tube theory of entangled polymer melts in the linear regime the stiffness length does not play a role,[45] except indirectly in the determination of the entanglement length and time scale.

What are the consequences of the increase in stiffness length for the resulting stress−strain relation? In a simple glassy system consisting of small molecules, no polymeric strain hardening takes place, but straining occurs at an approximately constant yield stress (apart from yield-peak effects at small strains), also seen in simulations.[41] Hence, if the stiffness length of the unperturbed polymer chain is of the order of the scale of the small molecules, then the increase in the effective stiffness length has not much effect on the total stress as this effect is overwhelmed by the background yield stress of the equivalent small-molecule system. As the stiffness length of unperturbed polystyrene is relatively small, it is plausible that this mechanism is at hand with polystyrene. The dominant initial nonaffine displacement is due to the phenyl ring side groups (as shown in section 9.3 and Figure 3); the nonaffine displacement of the backbone is much less. The increase in the effective stiffness length of the backbone will therefore not directly lead to much increase in total nonaffine displacement; consequently a small strain-hardening effect would be present.

If the stiffness length for the undeformed chain is, on the other hand, much larger, and the nonaffine displacements of the backbone atoms form a substantial part of the total nonaffine displacement, then the increase in the effective stiffness length does have an effect on the total nonaffine displacement. As a result, the stress will significantly increase at larger strains. If the stiffness length of the undeformed chain is so large that it is not much smaller than the entanglement length, the additional constraint from the entanglements could lead to an enhanced stiffening (similar to Langevin hardening[2]), an enhanced increase in the rate of nonaffine displacements and therefore to a larger strain-hardening modulus. However, it is not likely that this enhanced increase is applicable for PS in the studied strain range, since the contour length between entanglements is about 400 Å for this polymer,[46] substantially larger than its Kuhn length of 17 Å (appendix B.3). We therefore expect that entanglement effects are negligible for describing the strain hardening behavior of PS in the studied strain regime.

The picture of stiffening for a higher effective stiffness length is in accordance with some findings from literature. Stress−strain relations of preoriented samples[47] show a higher slope after initial yield than unoriented samples. Also in this case the maximal remaining extensibility is lower for the preoriented samples. Moreover, it was observed experimentally that polymers with a high Kuhn length tend to have a high value of G_h.[12]

A result found in ref 17 was that $G_h(\phi) = \phi G_h(1)$ with ϕ the monomer fraction of long chains (and $1 - \phi$ the monomer fraction of very short chains that do not show strain hardening). This could be interpreted as[17] that strain hardening was primarily the result of a more densely entangled melt for increasing ϕ (hence strain hardening would be caused by entanglements). However, the result can also be explained by the fact that the volume fraction of strain-hardening chains simply increases. Upon assuming that the total stress is the volume-fraction averaged sum of the stress of the pure individual components and assuming that each component can be described by eq 7 the result $G_h(\phi) = \phi G_h(1)$ is easily derivable without needing to refer to entanglements. It is, however, to be expected that it breaks down for entangled systems where a Gaussian description does not suffice.

6. Conclusions

In this study, we aim to find the microscopic mechanisms underlying the strain hardening effect, a pronounced increase in stress for large strains for polymeric glasses. By the support of a comparative simulation study of polystyrene and polycarbonate we acquire more insight in these mechanisms. For PC there is a pronounced increase in stress for large strains (strain hardening). For PS, conversely, this effect is much less prominent; the strain-hardening modulus of PS as simulated by the molecular-dynamics method is about half the value of that of polycarbonate. Our simulations thereby support the experimental results in which also a huge difference in the strain-hardening moduli is present. It is found that the rate of nonaffine displacement increases when the material is extended further. It was demonstrated earlier by ref 9 that the rate of changes in Lennard-Jones binding was linearly correlated with the stress. If one assumes that the rate of nonaffine displacement needed to strain the sample further increases if the rate of changes in LJ binding is higher (as a larger detour around the affine particle trajectory and thus more nonaffine displacement implies that more LJ bonds need to be broken to be able to make this detour), the conclusion must be that strain hardening is due to this increase in the rate of nonaffine displacement. This is in accordance with a measured quantitative correlation between the latter and the strain hardening modulus in the present study. The increase in the rate of nonaffine

displacement occurs because upon stretching the sample local chain parts (like covalent bonds and larger length scales) approach their maximal reasonable extensibility, requiring that larger length scales need to move nonaffinely for larger strains. It is shown that the nonaffine response of the intrachain length scales (such as noticed in ref 10 for a bead−spring model) and in the present study for both PS and PC can be understood in the picture that the effective stiffness length (here the stiffness length is determined by fitting the internal distances of the chain by the worm-like chain results; in the limit of an infinite chain the stiffness length coincides with the Kuhn length) of the perturbed chain increases with increasing strain. As the Kuhn length of polycarbonate is already larger than that of PS and the total nonaffine displacement of PC is to a large extent determined by the backbone atoms, the increase in the effective stiffness length leads to an increase in nonaffine displacement, more energy dissipation and hence a higher strain-hardening effect. For polystyrene the Kuhn length is small and the major part of nonaffine displacement is not caused by the backbone for the studied strain range. Hence the expected increase in the effective stiffness length during deformation does not lead to a substantial increase in plastic flow, so that at moderate strains PS behaves more like a simple glass without strain hardening, as opposed to polycarbonate.

Acknowledgment. Computational time was provided by the Stichting Nationale Computerfaciliteiten (NCF), with financial support from the Nederlandse Organisatie voor Wetenschappelijk Onderzoek (NWO). This research was also partly supported by NanoNed. AVL acknowledges the support of the Dutch Polymer Institute (DPI).

Appendix

A. Fully Extended Chain. There are many ways to determine the chain stiffness. One of them, fitting the root-mean-square end-to-end distance by the worm-like chain model (results in appendix B.3), requires information about the extended state. In the current appendix, we will determine this state.

Two methods will be employed to determine the dimensions of the fully-extended chain. The first one is to give a rough estimate of it by a simple calculation based on an all-trans configuration. In the second method the chain is forced to an extended state by means of molecular-dynamics simulations. This will serve as a check for the calculations.

A.1. Fully Extended All-Trans Chain. For polystyrene the maximal extension can be estimated as follows. The length of a backbone bond vector is on average approximately $l_{bb} = l_{CH_2-CH} = 1.53$ Å and the angle between subsequent backbone vectors equals $\theta_v = 180° - \theta_{CH-CH_2-CH} = 180° - \theta_{CH_2-CH-CH_2} = 70.5°$.[48] Hence the distance between two neighboring backbone CH units is $2l_{bb}\cos(\theta_v/2) = 2.5$ Å. If we assume that all backbone torsion angles are in the trans state (i.e., three subsequent bond vectors lie in a plane and are maximally separated), then $r_{n,\max,PS} = 1.25n$ Å (for an even number of backbone bonds n). However, this is only an approximation, as due to the phenyl-ring side group the stable trans state deviates from a planar configuration of three subsequent backbone bond vectors. The exact value of the trans state also depends on the type of dyad. These considerations render the maximally extended state slightly smaller in reality.

For polycarbonate a similar calculation for the length of the maximally extended chain can be carried out. If the carbonate group is in the (extended) trans state, then the monomer unit can be regarded as consisting of one long virtual bond of length $l_{vb} = 12.63$ Å.[49] The accompanying angle between two subsequent virtual-bond vectors is $\theta_v = 24.5°$. This makes the length of the cord vector connecting the centers of two adjacent virtual bonds equal to $l_{vb}\cos(\theta_v/2) = 12.3$ Å. Since a virtual bond consists of 12 backbone bonds, the maximal distance between two segments separated by n backbone bonds equals $r_{n,\max,PC} = 1.03n$ Å (for an even number of virtual bond vectors, i.e., if the number of backbone bonds n is a multiple of 24).

A.2. Fully Extended Chain Produced by Simulations. To check these all-trans-based model calculations, MD simulations are applied for determining the maximal extension of the polymer chains. We realize this by adding a very weak spring with potential $U_l = \frac{k_l}{2}(l - l_0)^2$ between the first and the last atom of a single polymer chain in vacuum, with l_0 a typical distance which is somewhat larger than the maximally extended state of the chain and l the instantaneous end-to-end distance of the chain. Then the force constant k_l of this extension spring is increased to drive the chain to its extended state. As the covalent bonds in the chain are modeled by stiff harmonic springs, their lengths are not constant and the chain could in principle be infinitely extended. In order to still be able to define a reasonable maximally extended state, an extra criterion is added, namely that the length of the covalent backbone bond should not increase more than 1/3 of the average fluctuation around the equilibrium value.

For the polystyrene chain this procedure is carried out at $T = 300$ K using l_0 equal to $1.25n$ Å, as the real extended dimension is anticipated to be less than this. Subsequently the force constant of the extension spring is increased until $k_l = 17$ kJ mol^{-1} Å^{-2} (and equilibrated shortly afterward for about 50 ps), as at this value the average length of the backbone bond is increased by 1%. This corresponds to about 1/3 of the relative fluctuation in the bond length $\frac{1}{\langle l \rangle}\sqrt{\langle \Delta l^2 \rangle}$ for the undeformed polymer chain in the glassy state at $T = 300$ K.

For the 10-monomer polycarbonate chain the same procedure is carried out. To achieve a similar relative extension of a similar backbone bond (the backbone bond between C and CT, see Figure 1 of ref 27 for the naming convention), the value of l_0 was set to 124 Å. Also for this chain the increase in the backbone bond (1%) is about one-third of the relative fluctuation of the same bond length for the isotropic case.

Summarizing this section, the end-to-end distance for the extended chain determined by the simulation method differs from the calculation by 2% for polycarbonate and less than 1% for polystyrene. This shows that despite the assumptions made in the calculations the final result is still reasonably accurate. The simulation results will, however, be used, as for shorter distances larger deviations do occur between the two methods.

B. Intrachain Length Scales of Vitrified Polystyrene and Polycarbonate. *B.1. Characteristic Ratio of Polystyrene.* The simulation results for the characteristic ratio for polystyrene together with the fits by eqs 3 and 4 are seen in Figure 10a). In the definition of the characteristic ratio a bond length l_b is needed. For PS l_b is taken to be the equilibrium length of a backbone C−C bond, $l_{b,PS} = 1.53$ Å.[50] The values for $\langle |\mathbf{r}_n|^2 \rangle / M_n$ are calculated by using $M_n = (n/n_{ch})M_{ch}$ where n_{ch} and M_{ch} are the total number of skeleton bonds and the total mass of a chain, respectively.

A few findings are apparent. The first is the long-chain limit. For our simulated polystyrene we find $C_\infty = 8.2$ at $T = 300$ K by using eq 3 as a fit and $l_{b,PS} = 1.53$ Å. This value is close to the (slightly larger) experimental values $C_\infty = 8.7-9.6$ from small-angle neutron scattering of a melt of polystyrene[51] at $T = 390-520$ K and $C_\infty = 9.9-10.2$, resulting from viscosity measurements

around 308 K for various solvents.[28] A different simulation result for a united-atom model of polystyrene is $C_\infty = 10.2$ at $T = 400$ K.[33] A local forcefield calculation gives $C_\infty = 11.0$.[52] Coarse-grained simulation results of PS are $C_{700} = 8$ at $T = 500$ K,[53] $C_{80} = 6.5$ at $T = 450$ K,[54] $C_\infty = 8.5$ at $T = 300$ K[55] and $C_\infty = 8.5$ at $T = 463$ K.[56]

Note that the ideal-chain fit formula, eq 4, would produce a much lower C_∞, namely 6.5. Although the range where the fit describes the data well is about the same for eqs 4 and 3, we can conclude that the melt-fit, eq 3, gives a more realistic estimate of C_∞.

The second finding is the functional behavior of the characteristic ratio. For short separations (small n) the characteristic ratio rises with increasing n, near $n = 25$ the maximum is achieved and for larger n it decreases again. This decrease is not to be expected for ideal chains. One might be tempted to think it is purely due to a bad equilibration at high temperature. Nevertheless, the equilibration of a PS chain at 600 K for more than 0.3 μs resulted in the same peak in C_n, while the average mean-square displacement of the atoms with respect to the center of mass of the chain exceeded twice the square radius of gyration of the chain. Such a peak in C_n is also found in a study of a melt of equilibrated relatively short chains.[57] The peak was shown to vanish for longer chains. One physical reason could be the stiffness-variation along the chain in a polymer melt[58] (the stiffness near the end of a chain can be much lower than in the middle). The peak may be somewhat more pronounced because of the temperature-dependence of the characteristic ratio of polystyrene[59,52] in combination with the finite cooling rate. To sum up, the characteristic ratio C_∞ of the simulated polystyrene is close to the experimental values.

B.2. Characteristic Ratio of Polycarbonate. The characteristic ratio is also calculated for the polycarbonate chains, see Figure 10b. For this polymer the monomer unit consists of different types of covalent backbone bonds, each with their own length. Instead of equaling l_b to an average covalent bond length, a longer virtual bond[28] is used, as long as it consists of a rigid object. The length of the virtual bond is not unique and different conventions are in use: $l_{b,PC} = 12.63$ Å for one virtual bond per monomer;[49] $l_{b,PC} = 8.65$ Å[60] or $l_{b,PC} = 7.0$ Å[61] for two virtual bonds per monomer. We will adopt $l_{b,PC} = 12.63$ Å. As a result we acquire in case of the melt-chain fit $C_\infty = 1.7$ and $\langle|\mathbf{r}|^2\rangle/M = 1.1$ Å^2 mol g^{-1} and in case of the ideal-chain fit $C_\infty = 1.4$ and $\langle|\mathbf{r}|^2\rangle/M = 0.80$ Å^2 mol g^{-1}. The experimental value for polycarbonate in a θ-solvent in which the intrinsic viscosity was converted to $\langle|\mathbf{r}|^2\rangle/M$[28,61] is $\langle|\mathbf{r}|^2\rangle/M = 0.87$ Å^2 mol g^{-1}. A configuration analysis says $\langle|\mathbf{r}|^2\rangle/M = 0.85$ Å^2 mol g^{-1}.[61] However, more recent small-angle neutron scattering experiments on polycarbonate melts give $\langle|\mathbf{r}|^2\rangle/M = 1.2-1.3$ Å^2 mol g^{-1} [62,63] and other configurational analysis models predict $\langle|\mathbf{r}|^2\rangle/M = 1.1$ Å^2 mol g^{-1} [64,65] and $\langle|\mathbf{r}|^2\rangle/M = 1.0$ Å^2 mol g^{-1}.[66,67] These results show that by making use of the melt-chain fit the experimentally measured melt-chain dimensions are reproduced in the case of polycarbonate.

B.3. Kuhn Lengths of PS and PC. Another way to compare the simulation results to the experimental values is to determine the stiffness length by mapping the results of $\langle|\mathbf{r}(L_c)|^2\rangle$ on the worm-like chain (eq 5). For an infinity long worm-like chain the stiffness length would then equal the Kuhn length. In order to map the two studied polymers on the worm-like chain the contour length is needed. As a contour length we could take the length in the maximally extended state. To correct for any errors in this length we assume that $L_{c,n} = \alpha r_{n,\max}$ with α a free fit parameter. A fit of $\langle|\mathbf{r}_n|^2\rangle/L_{c,n}$ vs $L_{c,n}$ for the two studied polymers onto the analogous expression for the worm-like chain (determined by eq 5) renders correction factor values $\alpha \approx 1.05$, i.e., the fitted contour length is about 5% larger than the maximal extension. The fitted values of the so-determined stiffness lengths are $l_{s,PS} = 12$ Å and $l_{s,PC} = 21$ Å if we confine the fit to the range $n = 1-40$.

Literature values for the Kuhn length are for polystyrene $l_K = 17$ Å and polycarbonate $l_K = 29$ Å.[60] In that reference these values were calculated by using the relation $l_K = l_b(1 + C_\infty)$. These literature values are higher than our simulation results if we use $l_s = l_K$. As the WLC has the same asymptotic behavior as the ideal-chain formula of C_n (eq 4) and both l_K and C_∞ are measurements of stiffness we can apply the discussion in sections B.1 and B.2 here as well. For example, the deviations are mainly caused by the relatively short chains we are studying. Other simulation results also demonstrate this, such as of some polyesters[68] and of the bond-fluctuation model.[69] Although our measured stiffness lengths are lower, they are so in a persistent way. Therefore the worm-like-chain fit is still valuable in studying changes in the stiffness length. The reason for using the WLC in the main text is that it leads to a better description of the chain structure at small scales and we want to use it for determining the stiffness length of the chains in the deformed samples.

To sum-up this appendix section, by means of MD simulations it is found that PC has a larger Kuhn or stiffness length than PS ($l_{s,PS} = 12$ Å and $l_{s,PC} = 21$ Å), thereby confirming the same trend in literature data. This is primarily caused by the phenyl rings within the backbone and the rigid backbone carbon in the propane group of PC. In this respect PC can be considered to be stiffer than PS.[63] Nevertheless, PC is is often considered to be a very flexible polymer.[61,70] This is because polycarbonate can be regarded as a nearly freely rotating chain albeit with a relatively large segment length. So with respect to the large virtual-bond length the chain is very flexible, as we found for the melt chain fit $C_\infty = 1.7$ (compared to PS, $C_\infty = 8.2$). With respect to a typical backbone-bond length, such as the length between two carbon atoms, the characteristic ratio is higher, making PC a stiffer chain.

Note Added After ASAP Publication. This article was published ASAP on July 15, 2009. Several typographical errors in section 5 of the manuscript have been corrected. The correct version was published on August 4, 2009.

Supporting Information Available: Text giving details on the polycarbonate force field used including figures showing its monomer unit and the bonded coordinates and a table giving the united force field data. This material is available free of charge via the Internet at http://pubs.acs.org.

References and Notes

(1) Haward, R. N.; Young, R. J. *The physics of glassy polymers*, 2nd ed.; Chapman & Hall: London, 1997.
(2) Treloar, L. R. G. *The physics of rubber elasticity*, 3rd ed.; Clarendon Press and Oxford University Press: Oxford, U.K., and New York, 2005.
(3) Ward, I. M.; Hadley, D. W. *An introduction to the mechanical properties of solid polymers*; John Wiley & Sons Ltd: West Sussex, England, 1993.
(4) Kramer, E. J. *J. Polym. Sci.: Polym. Phys.* **2005**, *43*, 3369–3371.
(5) van Melick, H. G. H.; Govaert, L. E.; Meijer, H. E. H. *Polymer* **2003**, *44*, 2493–2502.
(6) Salamatina, O. B.; Nazarenko, S. I.; Rudnev, S. N.; Oleinik, E. F. *Mech. Compos. Mater.* **1988**, *24*, 721–725.
(7) Oleinik, E. F.; Rudnev, S. N.; Salamatina, O. B.; Shenogin, S. V.; Kotelyanskii, M. I.; Paramzina, T. V.; Nazarenko, S. I. *e-Polym.* **2006**.
(8) Kremer, K.; Grest, G. S. *J. Chem. Phys.* **1990**, *92*, 5057–5086.

(9) Hoy, R. S.; Robbins, M. O. *Phys. Rev. Lett.* **2007**, *99*, 117801.
(10) Hoy, R. S.; Robbins, M. O. *Phys. Rev. E* **2008**, *77*, 031801.
(11) Haward, R. N. *Polymer* **1987**, *28*, 1485–1488.
(12) Haward, R. N. *Macromolecules* **1993**, *26*, 5860–5869.
(13) Govaert, L. E.; Tervoort, T. A. *J. Polym. Sci.: Polym. Phys.* **2004**, *42*, 2041–2049.
(14) Sarva, S. S.; Deschanel, S.; Boyce, M. C.; Chen, W. N. *Polymer* **2007**, *48*, 2208–2213.
(15) Boyce, M. C.; Arruda, E. M. *Polym. Eng. Sci.* **1990**, *30*, 1288–1298.
(16) Vorselaars, B.; Lyulin, A. V.; Michels, M. A. J. *J. Chem. Phys.* **2009**, *130*, 074905.
(17) Hoy, R. S.; Robbins, M. O. *J. Polym. Sci.: Polym. Phys.* **2006**, *44*, 3487–3500.
(18) McKechnie, J. I.; Haward, R. N.; Brown, D.; Clarke, J. H. R. *Macromolecules* **1993**, *26*, 198–202.
(19) Fetters, L. J.; Lohse, D. J.; Richter, D.; Witten, T. A.; Zirkel, A. *Macromolecules* **1994**, *27*, 4639–4647.
(20) Fetters, L. J.; Lohse, D. J.; Milner, S. T.; Graessley, W. W. *Macromolecules* **1999**, *32*, 6847–6851.
(21) Lyulin, A. V.; Vorselaars, B.; Mazo, M. A.; Balabaev, N. K.; Michels, M. A. J. *Europhys. Lett.* **2005**, *71*, 618–624.
(22) Angell, C. A. *Polymer* **1997**, *38*, 6261–6266.
(23) Capaldi, F. M.; Boyce, M. C.; Rutledge, G. C. *Phys. Rev. Lett.* **2002**, *89*, 175505.
(24) van Melick, H. G. H.; Govaert, L. E.; Meijer, H. E. H. *Polymer* **2003**, *44*, 3579–3591.
(25) Lyulin, A. V.; Balabaev, N. K.; Mazo, M. A.; Michels, M. A. J. *Macromolecules* **2004**, *37*, 8785–8793.
(26) Vorselaars, B.; Lyulin, A. V.; Michels, M. A. J. *Macromolecules* **2007**, *40*, 6001–6011.
(27) See the Supporting Information paragraph.
(28) Flory, P. J. *Statistical mechanics of chain molecules*; Hanser Publishers: Munich, Germany, 1989.
(29) Strobl, G. R. *The physics of polymers: concepts for understanding their structures and behavior*, 2nd ed.; Springer: Berlin; New York, 1997.
(30) Doi, M.; Edwards, S. F. *The theory of polymer dynamics*; Clarendon Press: New York, 1986.
(31) Wittmer, J. P.; Meyer, H.; Baschnagel, J.; Johner, A.; Obukhov, S.; Mattioni, L.; Müller, M.; Semenov, A. N. *Phys. Rev. Lett.* **2004**, *93*, 147801.
(32) Yerukhimovich, I. Y.; Irzhak, V. I.; Rostiashvili, V. G. *Vysokomol. Soyed.* **1976**, *A18*, 1470–1476.
(33) Han, J.; Boyd, R. H. *Polymer* **1996**, *37*, 1797–1804.
(34) Dutcher, J. R.; Marangoni, A. G. *Soft materials: structure and dynamics*; Marcel Dekker: New York, 2005.
(35) Although in uniaxial extension with zero external pressure the von Mises stress [71] equals the tensile stress, the fluctuations in the latter are higher for our simulations and we prefer to use the von Mises stress instead.
(36) Wendlandt, M.; Tervoort, T. A.; Suter, U. W. *Polymer* **2005**, *46*, 11786–11797.
(37) Tervoort, T. A.; Govaert, L. E. *J. Rheol.* **2000**, *44*, 1263–1277.
(38) Mulliken, A. D.; Boyce, M. C. *Int. J. Solids Structures* **2006**, *43*, 1331–1356.
(39) Ward, I. M.; Sweeney, J. *An introduction to the mechanical properties of solid polymers*, 2nd ed.; John Wiley & Sons Ltd: West Sussex, England, 2004.
(40) Capaldi, F. M.; Boyce, M. C.; Rutledge, G. C. *Polymer* **2004**, *45*, 1391–1399.
(41) Tanguy, A.; Leonforte, F.; Barrat, J. L. *Eur. Phys. J. E* **2006**, *20*, 355–364.
(42) Another definition of the nonaffine displacement is to compare the actual coordinate $\mathbf{r}(t_0 + t)$ with the affinely transformed coordinate at some initial time t_0 at zero strain, $\bar{\bar{F}}_{\mathrm{aff}} \cdot \mathbf{r}(t_0)$.[17] Here $\bar{\bar{F}}_{\mathrm{aff}}$ is the macroscopic deformation tensor.[72] Then one can construct a different nonaffine displacement $D_{na}(t)^2 = \langle (r(t_0 + t) - \bar{\bar{F}}_{\mathrm{aff}} \cdot \mathbf{r}(t_0))^2 \rangle$. The reason that we prefer the presented definition is illustrated by the following. Assume that a particle is initially situated in the origin at t_0 and that afterwards uniaxial extension starts. Assume further that it makes only one nonaffine jump from the origin to a new position in the extension direction, e.g., at t_1, and moves affinely afterwards. The nonaffine displacement of this particle therefore only takes place at t_1. Nevertheless, $D_{na}(t)^2$ keeps increasing for this particle even for times larger than t_1. The reason is that the nonaffine displacement is enlarged affinely after the jump at t_1 due to the ongoing extension of the sample. In the definition currently in use, the mean-square nonaffine displacement $\langle (\boldsymbol{r}_c(t_0 + t) - \boldsymbol{r}_c(t_0))^2 \rangle$ will not increase further, and therefore plastic events occurring in the initial stages of deformation will not be blown up.
(43) Vorselaars, B.; Lyulin, A. V.; Karatasos, K.; Michels, M. A. J. *Phys. Rev. E* **2007**, *75*, 011504.
(44) Casas, F.; Alba-Simionesco, C.; Montes, H.; Lequeux, F. *Macromolecules* **2008**, *41*, 860–865.
(45) Likhtman, A.; McLeish, T. *Macromolecules* **2002**, *35*, 6332–6343.
(46) Donald, A. M.; Kramer, E. J. *Polymer* **1982**, *23*, 1183–1188.
(47) ref 1., §5.2.7.
(48) Mondello, M.; Yang, H. J.; Furuya, H.; Roe, R. J. *Macromolecules* **1994**, *27*, 3566–3574.
(49) Sundararajan, P. R. *Macromolecules* **1987**, *20*, 1534–1539.
(50) Yoon, D. Y.; Sundararajan, P. R.; Flory, P. J. *Macromolecules* **1975**, *8*, 776–783.
(51) Boothroyd, A. T.; Rennie, A. R.; Wignall, G. D. *J. Chem. Phys.* **1993**, *99*, 9135–9144.
(52) Rapold, R. F.; Suter, U. W. *Macromol. Theor. Simul.* **1994**, *3*, 1–17.
(53) Milano, G.; Muller-Plathe, F. *J. Phys. Chem. B* **2005**, *109*, 18609–18619.
(54) Sun, Q.; Faller, R. *Macromolecules* **2006**, *39*, 812–820.
(55) Mulder, T.; Harmandaris, V. A.; V., L. A.; van der Vegt, N. F. A.; Vorselaars, B.; J., M. M. A. *Macromol. Theory Simul.* **2008**, *17*, 290–300.
(56) Mulder, T.; Harmandaris, V. A.; Lyulin, A.; van der Vegt, N. F. A.; J., M. M. A. *Macromol. Theory Simul.* **2008**, *17*, 393–402.
(57) Wittmer, J. P.; Beckrich, P.; Meyer, H.; Cavallo, A.; Johner, A.; Baschnagel, J. *Phys. Rev. E* **2007**, *76*, 011803.
(58) Schafer, L.; Elsner, K. *Eur. Phys. J. E* **2004**, *13*, 225–237.
(59) Kuwahara, N.; Saeki, S.; Konno, S.; Kaneko, M. *Polymer* **1974**, *15*, 66–68.
(60) Aharoni, S. M. *Macromolecules* **1983**, *16*, 1722–1728.
(61) Williams, A. D.; Flory, P. J. *J. Polym. Sci.: Polym. Phys.* **1968**, *6*, 1945–1952.
(62) Gawrisch, W.; Brereton, M. G.; Fischer, E. W. *Polym. Bull.* **1981**, *4*, 687–691.
(63) Ballard, D. G. H.; Burgess, A. N.; Cheshire, P.; Janke, E. W.; Nevin, A.; Schelten, J. *Polymer* **1981**, *22*, 1353–1354.
(64) Yoon, D. Y.; Flory, P. J. *Polym. Bull.* **1981**, *4*, 693–698.
(65) Laskowski, B. C.; Yoon, D. Y.; Mclean, D.; Jaffe, R. L. *Macromolecules* **1988**, *21*, 1629–1633.
(66) Lee, S.; Jeong, H. Y.; Lee, H. *Comput. Theoret. Polym. Sci.* **2001**, *11*, 219–226.
(67) Hutnik, M.; Argon, A. S.; Suter, U. W. *Macromolecules* **1991**, *24*, 5956–5961.
(68) Jung, B.; Schurmann, B. L. *Makromol. Chem-Rapid Commun.* **1989**, *10*, 419–425.
(69) Cifra, P. *Polymer* **2004**, *45*, 5995–6002.
(70) Berry, G. C.; Nomura, H.; Mayhan, K. G. *J. Polym. Sci.: Polym. Phys.* **1967**, *5*, 1–21.
(71) Lemaãitre, J.; Chaboche, J.-L. *Mechanics of solid materials*; Cambridge University Press: Cambridge, 1990.
(72) Macosko, C. W. *Rheology: principles, measurements, and applications*; Advances in interfacial engineering series; VCH: New York, 1994.